Inorganic Chemistry

ARTICLE

pubs.acs.org/IC

Mechanistic Insight into Olefin Epoxidation Catalyzed by Rhenium(V) Oxo Complexes That Contain Pyridazine-Based Ligands

Katrin R. Grünwald, Gerald Saischek, Manuel Volpe, and Nadia C. Mösch-Zanetti*

Institut für Chemie, Bereich Anorganische Chemie, Karl-Franzens Universität Graz, Schubertstrasse 1, A-8010 Graz, Austria

Supporting Information

ABSTRACT: Three novel tridentate pyridazine phenolate ligands were prepared in high yields by Schiff-base condensation of salicylic aldehyde with various pyridazine hydrazines (substituent R in the 6 position: R = Cl ($\mathbf{HL^{Cl}}$), ^{t}Bu ($\mathbf{HL^{t}Bu}$), or tol ($\mathbf{HL^{tol}}$)). They react with $[ReOCl_3(OPPh_3)(SMe_2)]$ to form rare mononuclear *trans*-dichloro oxo complexes of general formula $[ReOCl_2(L^R)]$ with R = tol (**1**), ^{t}Bu (**2**), or Cl (**3**) as confirmed by single-crystal X-ray diffraction analyses of **1** and **2**. They were found to be catalysts for oxidation of cyclooctene to the corresponding epoxide by *tert*-butyl hydroperoxide (TBHP). Extensive UV−vis and NMR spectroscopic investigations followed by evaluation using the powerful Mauser method revealed mechanistic details. This showed the catalyst precursor $[ReOCl_2(L)]$ (**2**) to be transformed into the rhenium(VII) compound $[ReO_3L]$ (**4**) in a two-step reaction via intermediate **INT** which is tentatively assigned to $[ReO_2L]$. Confirmation gave the isolation of **4** by reaction of **2** with excess of TBHP. Monitoring the catalytic oxidation reaction by UV−vis spectroscopy clearly excludes the two rhenium(V) compounds **2** and **INT** from being the catalytically active species as their formation is several orders of magnitude faster than the observed catalytic epoxidation reaction.

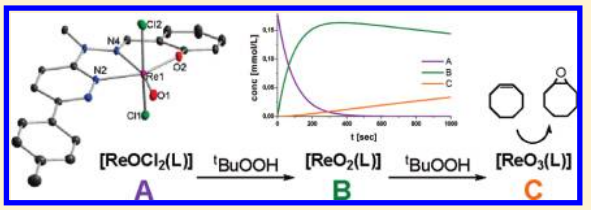

INTRODUCTION

Rhenium oxo complexes made their way from mere curiosities to catalysts for various organic transformations.[1−3] In particular, methylrhenium trioxide (MTO) was found to be, after its serendipitous discovery,[4] a highly versatile, robust, and active Re(VII) oxidation catalyst.[5,6] Applying various oxygen donors such as bis(trimethylsilyl) peroxide,[7] a urea−hydrogen peroxide complex,[8] or substituted pyridines[9] in combination with the green oxidant H_2O_2 led to the huge success of MTO and derivatives thereof.[10] Furthermore, side reactions[11] as well as the influence of inorganic and metal−organic cocatalysts on the catalytic oxidation processes applying MTO are thoroughly investigated.

Rhenium(V) oxo complexes are far less explored, although their use provides several advantages. They are prepared in a straightforward manner and are usually air-stable solids. Rhenium(V) oxo complexes are active catalysts in a number of oxidation and reduction processes.[12−14] In particular, several oxygen-atom transfer (OAT)[15,16] and epoxidation reactions attracted significant interest.[17−24] First, rhenium(V) oxidation catalysts feature salen-derived ligands,[25] which inspired the development of related systems with high catalytic activities.[26] However, the investigated Re(V) epoxidation catalysts do not reach as yet the high activity observed with Re(VII). Further exploration of novel rhenium(V) compounds in oxidation reactions is thus in need. Here, we present a series of salen-derived monoanionic ligands containing a pyridazine moiety, similar to those we reported recently.[27] The heterocycle belongs to the electron-deficient group, in contrast to pyridine, so that we expected unusual electronic influences on the coordinating capability as well as on the catalytic activity. Furthermore, the lone pair located at the noncoordinating nitrogen atom may additionally interact as it provides electrons for hydrogen bonding and may thus help in stabilizing intermediate species. Herein, we report the preparation of air-stable Re(V) complexes of the type $[ReOCl_2(L)]$ exhibiting a rare *trans*-dichloro configuration and their application in epoxidation catalysis. During our studies we gained further insight into the role of Re(V) as a precatalyst in oxidation reactions.

RESULTS AND DISCUSSION

Synthesis of the Ligands. The three tridentate pyridazine-containing phenol ligands HL^R (R = *p*-tolyl, $\mathbf{HL^{tol}}$, R = *tert*-butyl, $\mathbf{HL^{tBu}}$, R = chloro, $\mathbf{HL^{Cl}}$) employed in this report were prepared by Schiff-base condensation of unsymmetrically substituted pyridazine hydrazines with salicylic aldehyde in ethanol in quantitative yields and high purities. The pyridazine hydrazine precursors were synthesized by a convenient method we recently described.[27] Ligands $\mathbf{HL^{tol}}$, $\mathbf{HL^{tBu}}$, and $\mathbf{HL^{Cl}}$ were characterized by NMR spectroscopy, which confirmed the structure shown in Scheme 1. The ligands were obtained as off-white crystalline solids, which were well soluble in polar solvents at elevated temperatures but displayed limited solubility at room temperature or in apolar solvents.

Synthesis of the Complexes. Complex synthesis was carried out by stirring an acetone suspension of stoichiometric amounts of the respective ligand and $[ReOCl_3(OPPh_3)(SMe_2)]$[28] at 50 °C. After completion of the reaction, indicated by complete dissolution of the starting material, the deep red solutions were

Received: April 12, 2011
Published: July 07, 2011

   dx.doi.org/10.1021/ic200756r | *Inorg. Chem.* 2011, 50, 7162–7171

Scheme 1. Synthesis of Ligands HL^{tol}, HL^{tBu}, and HL^{Cl} and Complexes of the Type $[ReOCl_2(L^R)]$ (R = tol (1), ^{t}Bu (2), Cl (3))

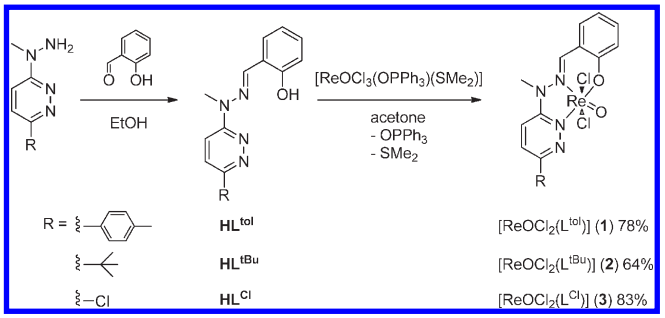

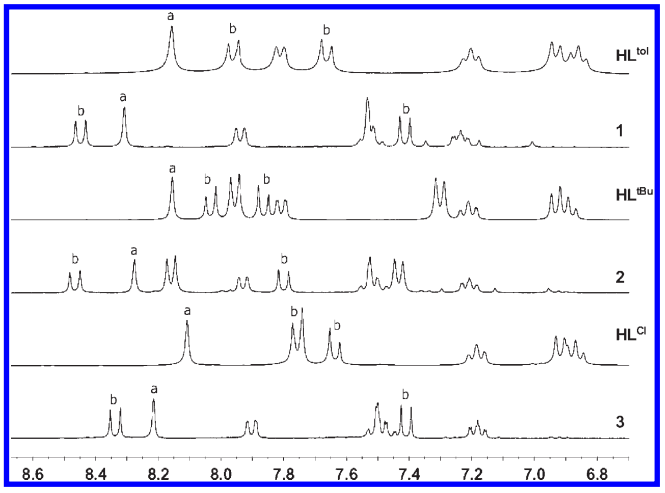

Figure 1. ^{1}H NMR spectra (aromatic region in DMSO-d_6) of HL^{tol}, $[ReOCl_2(L^{tol})]$ (**1**), HL^{tBu}, $[ReOCl_2(L^{tBu})]$ (**2**), HL^{Cl}, and $[ReOCl_2(L^{Cl})]$ (**3**): (a) imino proton resonance, (b) pyridazine resonances, other resonances can be assigned to the protons of the phenolate ring.

filtered and allowed to cool to room temperature. Upon evaporation of the solvent dark auburn crystalline materials were obtained. Recrystallization from hot acetonitrile or dichloromethane gave complexes $[ReOCl_2(L^R)]$ (R = tol (**1**), ^{t}Bu (**2**), and Cl (**3**)) in good yields as dark red crystals. Those of compounds **1** and **2** were suitable for X-ray diffraction analysis (vide infra). All complexes are moderately soluble in a number of common solvents such as methanol, acetonitrile, or acetone, fairly soluble in THF or dichloromethane, and insoluble in diethyl ether and pentane. The *tert*-butyl group in compound **2** increases the solubility.

The compounds were characterized by ^{1}H NMR spectroscopy. Most protons in the molecules are found in the aromatic region (phenol, pyridazine, and imine) which leads to rather crowded spectra in this region. However, in the ^{1}H NMR spectra the two doublets of the pyridazine protons and the singlet of the imino proton are distinct as shown in Figure 1. Furthermore, those resonances are significantly shifted upon coordination of the ligand, rendering them a convenient tool for characterization. Figure 1 shows a comparison of the aromatic regions of the uncoordinated ligand and of the corresponding rhenium compound for each individual couple. In all cases, the imino resonances

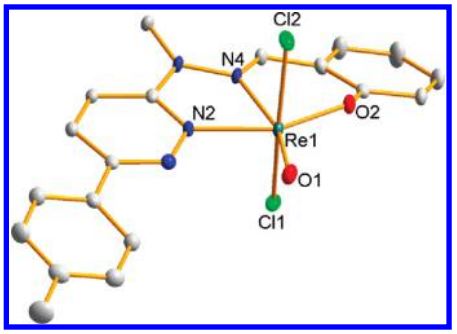

Figure 2. Molecular structures of complex **1** (50% probability). Hydrogen atoms and solvent molecules have been omitted for clarity.

are shifted downfield upon coordination (Figure 1, a). The two corresponding doublets of the pyridazine ring are shifted apart between 0.2 and 0.4 ppm in the uncoordinated ligand, whereas coordination leads to increased shift differences between the two ($\Delta\delta$ = 0.8 to 1 ppm) induced by coordination to the metal (Figure 1, b). All protons of the phenolate rings experience a downfield shift except one doublet of doublets, whose shift remains almost constant for all complexes upon coordination to the metal center.

Molecular Structures of the Complexes. For complexes **1** and **2** single crystals suitable for X-ray diffraction analysis were obtained by recrystallization from acetonitrile and dichloromethane, respectively. A representative molecular view of complex **1** is given in Figure 2 (a molecular view of complex **2** is included in the Supporting Information, Figure S1), selected bond lengths and angles are in Table 1, and crystallographic data are in Table 2.

Complexes **1** and **2** are isostructural and show distorted octahedral geometries around the Re centers. The planar ligands coordinate in a tridentate meridional mode, while the oxo groups are trans to the imino nitrogen (N4) atoms completing the basal plane. The chlorine atoms occupy the apical positions of the octahedron and are thus trans to each other, albeit distorted (Cl1−Re1−Cl2 166.60(2)° in **1** and 165.72(8)° in **2**). This configuration is rare. To the best of our knowledge, this is the first oxo *trans*-dichloro rhenium crystal structure featuring a tridentate N_2O ligand. Comparable systems featuring a N_2O donor set form mononuclear[29−32] as well as oxo-bridged dimeric structures.[29,30,33,34] All of these systems involve simple heterocyclic nitrogen donors such as pyridine or pyrimidine. In addition, one bidentate N_2[35] and one tetradentate N_4 ligand[36] are reported, which form complexes with the *trans*-dichloro oxo configuration. In the starting material $[ReOCl_3(OPPh_3)(SMe_2)]$[28] the three chlorine atoms are coordinated in a meridional mode.[37] Thus, this precursor presents easy access to rare Re^V *trans*-dichloro oxo complexes. In complexes **1** and **2** the N2−Re1−O2 angle deviates significantly from the ideal geometry, being 155.18(7)° and 155.68(18)°, respectively. Although the structures were measured at different temperatures (100 K for **1** and 293 K for **2**), the rhenium oxygen bonds Re1−O1 are comparable, being 1.6734(17) and 1.656(3) Å for **1** and **2**, respectively, confirming a triple-bond character.[38] The Re−O2 bonds are 1.9358(15) and 1.930(3) Å for **1** and **2**, respectively, similar to those reported in the literature.[17,18,39,40] The pyridazine N2−Re1 bond is shorter than the imino N4−Re1 bonds, which is in agreement with the trans influence induced by O1. Both apical chloro ligands display bond distances to the central metal similar to those reported in the literature.[29−32]

dx.doi.org/10.1021/ic200756r |*Inorg. Chem.* 2011, 50, 7162–7171

Table 1. Selected Bond Lengths [Å] and Angles [deg] for Complexes [$ReOCl_2(L^{tol})$] (1) and [$ReOCl_2(L^{tBu})$] (2)

	1	2		1	2
Re1−O1	1.6734(17)	1.656(3)	Re1−N4	2.2056(19)	2.201(3)
Re1−O2	1.9358(15)	1.930(3)	Re1−Cl1	2.3746(6)	2.337(5)
Re1−N2	2.0909(18)	2.095(3)	Re1−Cl2	2.3787(6)	2.379(5)
O1−Re1−O2	113.46(7)	112.22(14)	N2−Re1−Cl1	94.44(5)	92.3(4)
O1−Re1−N2	91.19(8)	91.56(14)	N4−Re1−Cl1	82.63(5)	84.6(3)
O2−Re1−N2	155.18(7)	155.68(18)	O1−Re1−Cl2	96.61(7)	97.5(5)
O1−Re1−N4	163.42(8)	164.00(13)	O2−Re1−Cl2	85.04(5)	80.3(4)
O2−Re1−N4	83.02(7)	83.73(13)	N2−Re1−Cl2	89.42(5)	92.0(3)
N2−Re1−N4	72.48(7)	72.45(12)	N4−Re1−Cl2	86.32(5)	83.7(3)
O1−Re1−Cl1	96.13(6)	96.0(5)	Cl1−Re1−Cl2	166.60(2)	165.72(8)
O2−Re1−Cl1	86.10(5)	90.3(4)			

Table 2. Crystallographic Data and Structure Refinement for Complexes 1 and 2

	$1\cdot 2C_2H_3N$	$2\cdot CH_2Cl_2$
empirical formula	$ReC_{19}H_{17}Cl_2N_4O_2\cdot 2(C_2H_3N)$	$ReC_{16}H_{19}Cl_2N_4O_2\cdot CH_2Cl_2$
M_r, g/mol	672.57	641.38
cryst description	tablet, black	tablet, red
cryst syst	monoclinic	orthorhombic
space group	$C2/c$	$Pna2_1$
a, Å	29.2128(15)	18.639(3)
b, Å	13.7694(7)	15.233(2)
c, Å	14.0722(7)	7.9877(11)
α, deg	90.00	90.00
β, deg	114.230(2)	90.00
γ, deg	90.00	90.00
volume, Å^3	5161.8(5)	2267.9(5)
Z	8	4
T, K	100(2)	293(2)
D_c, g/cm^3	1.731	1.878
μ, mm^{-1}	1.407	1.407
F(000)	2624	1240
reflns collected	32 563	26 521
unique reflns	7516	6200
reflns with $I \geq 2\,\sigma\,(I)$	6499	5048
R(int), $R(\sigma)$	0.0453, 0.0302	0.0430, 0.0377
no. of parameters/restraints	311/0	228/7
final $R1$ [a], $wR2$ [b] ($I \geq 2\,\sigma$)	0.0206, 0.0488	0.0301, 0.0659
R indices (all data)	0.0283, 0.0532	0.0441, 0.0715
GOF on F^2	1.060	1.016
largest diff. peak and hole, e/Å^3	1.603, −1.110	1.271, −0.875

[a] $R1 = \Sigma||F_o| - |F_c||/\Sigma|F_o|$. [b] $wR2 = \{\Sigma[w(F_o^2 - F_c^2)^2]^2/\Sigma[w(F_o^2)^2\}^{1/2}$.

Electrochemical Studies. Redox properties of complexes **1**−**3** were investigated by cyclic voltammetry in dry acetonitrile solution (Table 3). All complexes show fully reversible oxidation waves with half-wave potentials of 0.869 V for **1**, 0.851 V for **2**, and 0.932 V for **3**, which can be assigned to one-electron oxidations $Re^V \rightarrow Re^{VI}$. The trend of the potentials (*tert*-butyl (**2**) < tolyl (**1**) < chloride (**3**)) is consistent with the electronic nature of the substituents at the pyridazine ring. Electron-withdrawing groups (Cl, tol) decrease and the electron-donating *tert*-butyl group increases the electron density at the metal, rendering the latter more easy to oxidize. The reversibility prompted us to investigate chemical oxidations of **1**−**3** with various strong one-electron oxidation agents ($[NO]^+$, $[thianthrene]^{+\cdot}$ or antimony halide),[41] forming a potential Re^{VI} species. However, only decomposition products were obtained, presumably due to side reactions in the ligand backbone.

All complexes show irreversible reductions waves at −1.159 V for **1**, −1.179 for **2**, and −1.102 V for **3** following the expected trend of the potentials (chloride (**3**) < tolyl (**1**) < *tert*-butyl (**2**)), where the electron-donating *tert*-butyl system is more difficult to reduce.

Catalytic Epoxidations. Our ongoing interest in epoxidation reactions employing Re(V) compounds[17−19] led us to explore also compounds **1**−**3** as catalysts in the epoxidation of *cis*-cyclooctene with *tert*-butyl hydroperoxide (TBHP) as the oxidant. This model reaction (Scheme 2) allowed us to compare the performance the pyridazine complexes to the few previously investigated Re(V) systems.[17−24] Rhenium(V) compounds are potentially ideal catalysts as they are conveniently prepared and are easy to handle in ambient conditions. In particular, the latter would be advantageous over Re(VII) systems that tend to be more difficult to handle.

Typically, the catalyst (1 equiv) and *cis*-cyclooctene (100 equiv) were mixed in chloroform and heated to 50 °C, whereupon the catalyst slowly dissolved. The oxidant (TBHP in *n*-decane, 200 equiv) was then added, which initiated the reaction. The reaction performance was monitored by periodically taking samples for GC-MS analysis (Table 4). Complexes **1**−**3** convert the substrate into epoxide; no other products were analyzed. Despite the limited solubility of the complexes in chloroform at room temperature, good performances could be achieved at 50 °C. At temperatures lower than 50 °C no conversion was observed. Employing solvents in which compounds **1**−**3** are more soluble, such as acetonitrile or acetone, did not yield any product. Furthermore, with other potential substrates such as cyclohexene or 4-phenyl butane no conversion was observed.

The performance of catalysts **1**−**3** is in the same range as previously investigated active Re^V systems.[17−24] The lower conversion of the olefin after 0.25 h employing complex **3** can be attributed to its lower solubility compared to **1** and **2**. In order to obtain more insights into the mechanism we decided to explore the catalyst in more detail. Whereas mechanistic information has elegantly been elucidated for Re(VII) catalysts,[42−44] no information on the catalytically active species of the Re(V) systems is as yet

dx.doi.org/10.1021/ic200756r |*Inorg. Chem.* 2011, 50, 7162–7171

Table 3. Electrochemical Data for 1−3 in Dry Acetonitrile Solution at Room Temperature[a]

compound	E^{p}_{red}	$E^{1/2}_{ox}$	ΔE^{p}	process
$[ReOCl_2(L^{tol})]$ **1**	−1.159			$Re^{V} \rightarrow Re^{IV}$
		0.869	75	$Re^{V} \rightarrow Re^{VI}$
$[ReOCl_2(L^{tBu})]$ **2**	−1.179			$Re^{V} \rightarrow Re^{IV}$
		0.851	77	$Re^{V} \rightarrow Re^{VI}$
$[ReOCl_2(L^{Cl})]$ **3**	−1.102			$Re^{V} \rightarrow Re^{IV}$
		0.932	71	$Re^{V} \rightarrow Re^{VI}$

[a] Measured by cyclic voltammetry in CH_3CN at 50 mV/s. *E* vs $Ag/AgNO_3$. Conditions: Pt disk (working), Pt wire (counter), and $Ag/AgNO_3$ (reference) electrodes; supporting electrolyte 0.05 M TBAP solution in CH_3CN in an Ar atmosphere.

available. Such information would be helpful for development of future Re^{V} precursors that show superior performance.

UV−Vis Spectroscopy Under Catalytic Conditions. In order to gain insight into the formation of the catalytically active species time-resolved UV−vis measurements were performed. Only the *tert*-butyl-substituted compound **2** exhibits solubility in chloroform which was high enough for the investigations. With the help of stock solutions, 0.2 μmol of compound **2** (1 equiv), 20 μmol of *cis*-cyclooctene (100 equiv), and 2 g of chloroform were mixed in a quartz cuvette, which was placed into a spectrometer equipped with a holder thermostat controlled at 50 °C. In order to increase the rate of the diluted reaction, excess oxidation reagent was added (800 μmol of TBHP, 4000 equiv). Immediately after addition of TBHP the first UV−vis spectrum was measured, and thereafter, every 5 min additional spectra were acquired for up to 9 h. Figure 4 shows UV−vis spectra between 300 and 400 nm. The first spectrum (in bold) shows a strong absorption at 355 nm which decreases with time. New absorptions at 307 and 335 nm appeared during the first 5 min, after which they decrease to give a final spectrum after 3 h without distinct absorption bands in this region (see insert, Figure 4).

These results suggest that the catalyst precursor **2** converts quickly into at least one intermediate species **INT** (absorptions at 307 and 335 nm) but with time slowly reacts further to a final product. To monitor epoxide formation during the reaction, GC-MS samples were taken periodically (Figure 4 b). Both the starting material **2** and **INT** do not seem to be the catalytically active compounds as no correlation to the rate of the catalytic reaction is observable.

We were interested in the nature of the formed compounds, in particular in the intermediate species immediately formed after addition of the peroxide as well as in the species formed after prolonged reaction time. By comparing literature data, it seems reasonable to assign the UV−vis absorption at 335 nm and thus the intermediate species **INT** to a rhenium *trans*-dioxo compound, as comparable complexes absorb in the same wavelength range ($[Re(O)_2(py)_4]^+$ λ_{max} = 331 nm,[45] $[Re(O)_2(4\text{-MeOPy})_4]^+$ and $[Re(O)_2(4\text{-pyrrolidinopyridine})_4]^+$ λ_{max} = 334 nm,[46] $[Re(O)_2(\text{acyclic tetraamine})]^+$ λ_{max} = 350 nm,[47] $[Re(O)_2(\text{tridentate } SO_2 \text{ ligand})]$ λ_{max} = 300−350 nm,[48] or $[Re(O)_2(\text{bis-(3,5-dimethylpyrazol-1-yl)methane})]^+$ λ_{max} = 303 nm[49]). In contrast, $[Re(O)_3Br(phen)]$, an analogue to a potentially oxidized product, shows exclusively absorption below 300 nm.[50]

In order to gain further insight into the nature of the compounds the reactivity of compound **2** with excess TBHP without substrate was investigated by ^{1}H NMR, IR, and UV−vis spectroscopies.

Scheme 2. Catalytic Epoxidation of Cyclooctene[a]

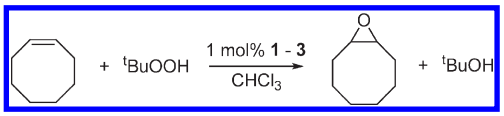

[a] Conditions: 1 mol % Re catalyst **1**−**3**, 1 equiv of cyclooctene, 2 equiv of ^{t}BuOOH (5.5M in decane), 50 °C, $CHCl_3$.

Table 4. Catalytic Performance of Complexes 1−3[a]

catalyst	time [h]	cyclooctene [%]	cyclooctene oxide [%]
$[ReOCl_2(L^{tol})]$ (**1**)	0.25	67	33
	4	55	45
	24	45	55
$[ReOCl_2(L^{tBu})]$ (**2**)	0.25	72	28
	4	58	42
	24	44	56
$[ReOCl_2(L^{Cl})]$ (**3**)	0.25	87	13
	4	35	65
	24	34	66

[a] Reactions were performed in chloroform at 50 °C, 1 equiv of substrate (cyclooctene), 1 mol % catalyst, 2 equiv of TBHP. GC-MS analysis, internal standard *n*-decane.

Oxidation of Compound 2: NMR and IR Spectroscopies. Reaction of complex **2** with TBHP in the absence of substrate was investigated by ^{1}H NMR spectroscopy. In a vial, 20 mg of complex **2** (36 μmol) was reacted with TBHP (10 equiv, 360 μmol) in 2 mL of chloroform at 50 °C. After 8 h product **4** was isolated as a pale orange solid material by removing all volatiles. Its UV−vis spectrum was identical to the final spectrum of the UV−vis experiment shown in Figure 4 a. The ^{1}H NMR spectrum in DMSO-d_6 showed one new set of downfield-shifted ligand signals with respect to the resonances of the starting complex **2** (aromatic region shown in Figure 5).

The two doublets marked with (a) are typical for the two pyridazine protons whereas (b) corresponds to the imino resonance. Those three signals are remarkably deshielded by $\Delta\delta$ = 1.0, 0.5, and 2.25 ppm, respectively, in comparison to **2**. The strong downfield shift of an imino resonance has previously been explained by the strong trans influence of an oxo ligand.[51] Due to solubility reasons, no meaningful ^{13}C NMR spectrum could be obtained. Furthermore, in the IR spectrum of the isolated material of complex **4** a very strong absorption at ν = 888 cm^{-1} was observed. Very strong absorptions in this region are typical for rhenium trioxo complexes (e.g., $[ReO_3Br(phen)]$, $[ReO_3Cp]$, and $[ReO_3(tacn)]^+$ at 906, 887, and 878 cm^{-1}).[50,52] Thus, NMR and IR spectroscopies let us believe complex **4** to be the oxidized rhenium trioxo complex $[ReO_3(L^{tBu})]$, which is formed via the proposed intermediate **INT** (eq 1).

$$\underset{\mathbf{2}}{[ReOCl_2(L^{tBu})]} \xrightarrow{+^{t}BuOOH} \underset{\text{proposed INT}}{[ReO_2(L^{tBu})]} \xrightarrow{+^{t}BuOOH} \underset{\mathbf{4}}{[ReO_3(L^{tBu})]} \quad (1)$$

dx.doi.org/10.1021/ic200756r |*Inorg. Chem.* 2011, 50, 7162–7171

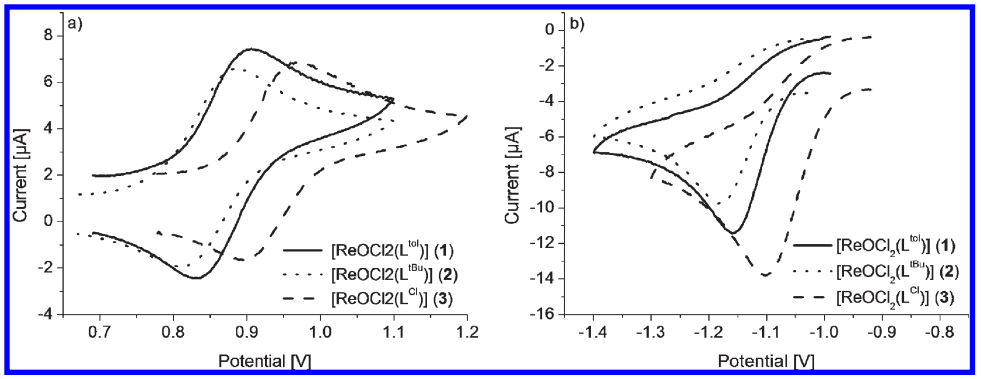

Figure 3. Cyclic voltammogram of complexes **1**−**3** in acetonitrile solution (scan rate 50 mV/s): (a) reversible oxidations and (b) irreversible reductions.

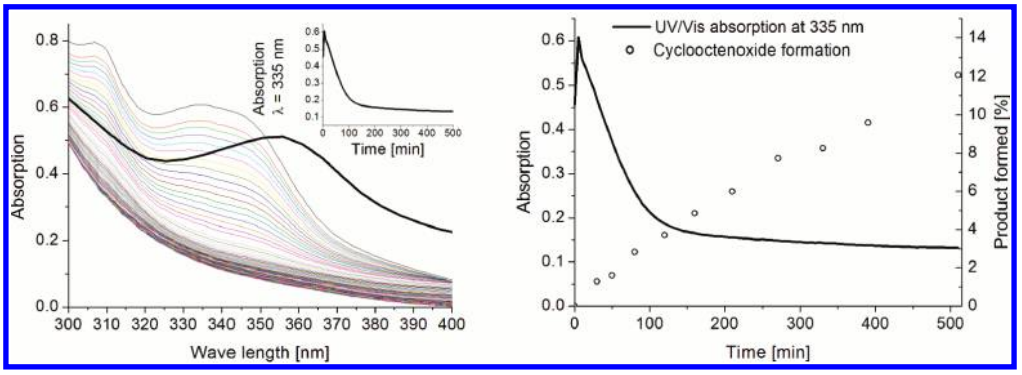

Figure 4. Catalytic epoxidation of cyclooctene, 1 mol % catalyst **2**, 1 equiv of cyclooctene, 40 equiv of TBHP. (a) UV−vis spectra measured every 5 min. The initial spectrum is marked with a bold line. The insert shows the absorbance at 335 nm. (b) Product formation (GC-MS) and UV−vis absorbance at 335 nm.

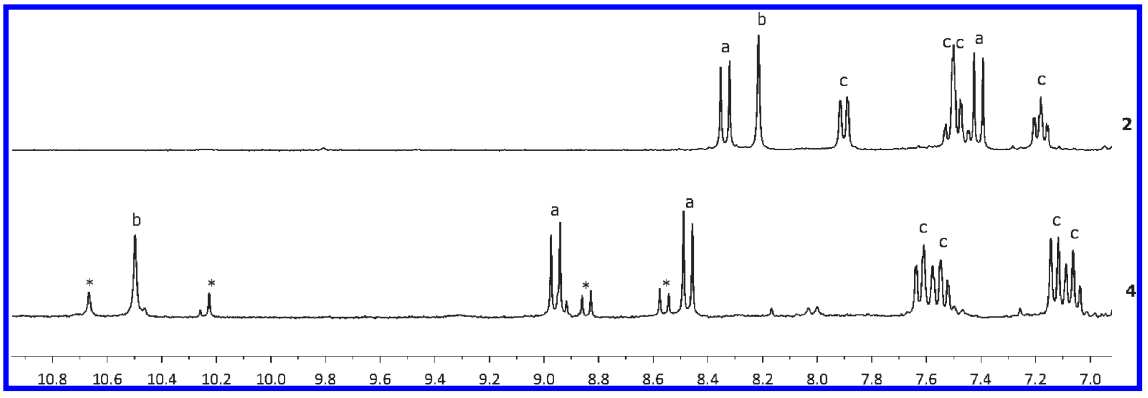

Figure 5. ^{1}H NMR spectra (aromatic region in DMSO-d_6) of [$ReOCl_2(L^{tBu})$] (**2**) and the crude product (**4**) obtained after reaction with 10 equiv of TBHP after 8 h: (a) pyridazine resonances, (b) imino signal, (c) aromatic phenolate signals. Asterisks (*) marked unidentified impurities.

Oxidation of Compound 2: UV−Vis Spectroscopy. Oxidation of compound **2** with excess TBHP was followed by UV−vis spectroscopy. This allows further insight into the reaction mechanism by quantifying the number of reaction components in solution without the need to isolate the individual species.

When we performed time-resolved UV−vis spectroscopy of the reaction solution with an excess of TBHP (19 equiv) in the absence of the substrate (Figure 6), an identical behavior was observed as in the catalytic reaction (see Figure 4). These data were subjected to graphical and mathematical assessment in order to elucidate the number of linearly independent reaction steps involved in formation of complex **4**.

For detailed investigation the region from 300 to 350 nm was considered, as there the largest absorption changes occur during the reaction. Prior to the rate equation establishment the sum of independent reactions in the system has to be determined. This analysis was done graphically according to Mauser as well as numerically with singular value decomposition (SVD)[53,54] of the experimental matrix $A_{\lambda t}$. Processing details are summarized in the Supporting Information.

dx.doi.org/10.1021/ic200756r |*Inorg. Chem.* 2011, 50, 7162–7171

Graphical Assessment According to Mauser.[53,54] The A diagram (A/A) and the A difference diagram (AD/AD) for selected wavelength combinations show curved lines as depicted in Figure 7a and 7b, whereas the absorbance−difference plot (ADQ) represents straight lines with high correlation to linear fits as demonstrated in Figure 8.

The three-dimensional representation of the absorbance−absorbance−absorbance correlation results in a curve laying onto a plane. Rotation of the coordinate system leads to projection of the plane as shown in Figure 9.[55] Graphical evaluation of the data according to Mauser thus results in a reaction system of two independent steps.

Numerical Assessment.[56,57] The number of the linear independent reactions is determined by the rank of the data matrix A applying the SVD method. The diagonal matrix S obtained from the transformation $A = USV^T$ consists of a series of singular values (Figure 10). As the calculations are based on real data, introduction of a tolerance (0.005) is essential. Thus, on applying SVD to the six selected wavelengths (305−340 nm), two singular values can be obtained, which clearly indicate a reaction system consisting of two independent steps.

Both evaluations agree; thus, an irreversible reaction system with two steps is anticipated for the present process. From the chemistry involved, it is also clear that the reaction must be a consecutive reaction. A reaction in two parallel steps is excluded. Due to the excess of TBHP as the oxidizing agent pseudo-first-order conditions are obeyed.

$$A + [B] \rightarrow C \rightarrow D$$

Fitting experimental data[58] (e.g., 315 nm) to equation S6 (Supporting Information) provided the reaction constants $k_1 = 1.047 \times 10^{-2}\ s^{-1}$ and $k_2 = 1.770 \times 10^{-4}\ s^{-1}$. Experimental data and calculated values agree well as shown in Figure 11.

Additionally, experimental data with strong absorption variation (from 305 to 360 nm) were fitted applying the Levenberg−Marquardt algorithm (least-squares fit), yielding experimental rate constants $k_1 = 1.06 \pm 0.02 \times 10^{-2}\ s^{-1}$ and $k_2 = 2.3 \pm 0.8 \times 10^{-4}\ s^{-1}$.

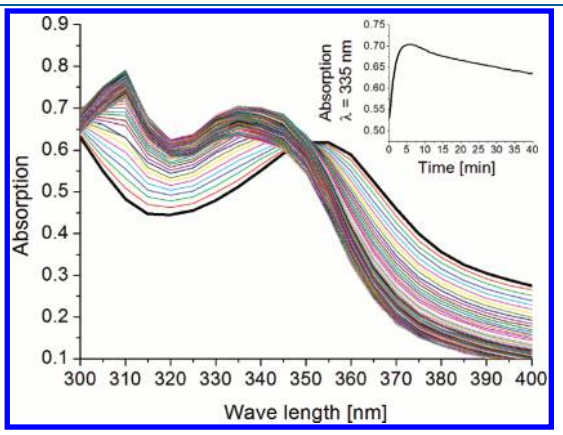

Figure 6. Oxidation of complex **2** (1 equiv) with 19 equiv of TBHP. UV−vis spectra measured every 8 s. The initial spectrum is marked with a bold line. (Insert) Absorption at 335 nm vs time.

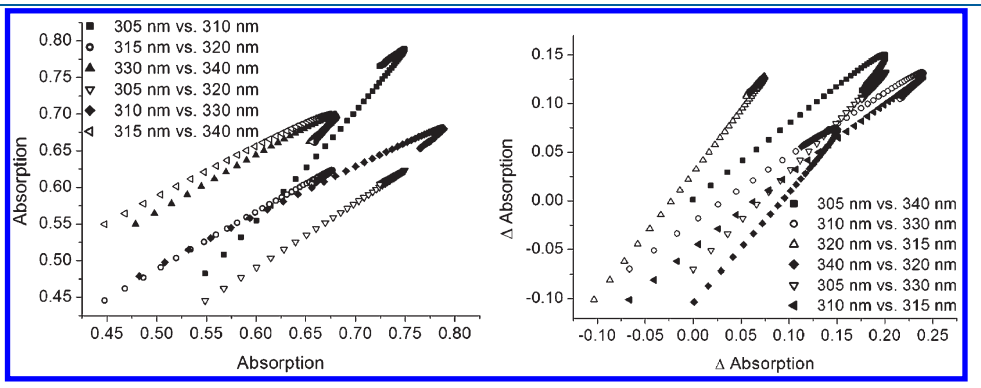

Figure 7. (a) Extinctions plot. (b) Differential extinctions plot.

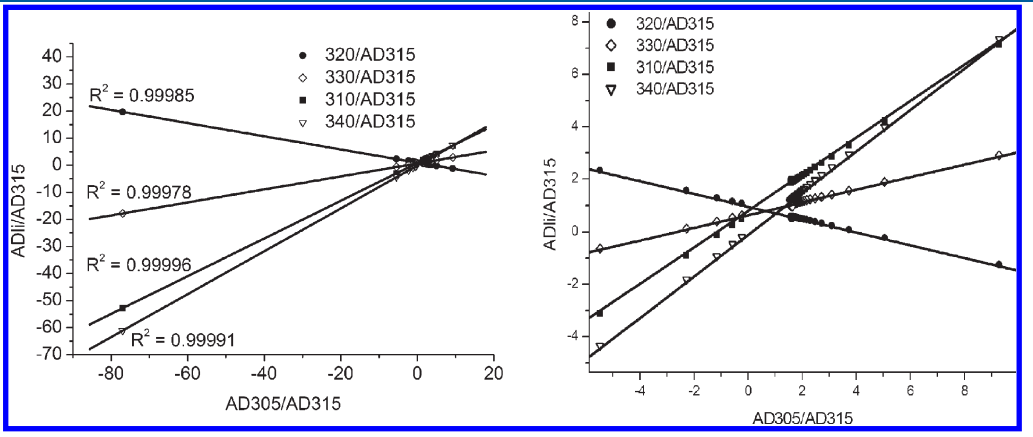

Figure 8. ADQ plot for selected wavelengths; full scale (left) and zoom (right).

dx.doi.org/10.1021/ic200756r |*Inorg. Chem.* 2011, 50, 7162–7171

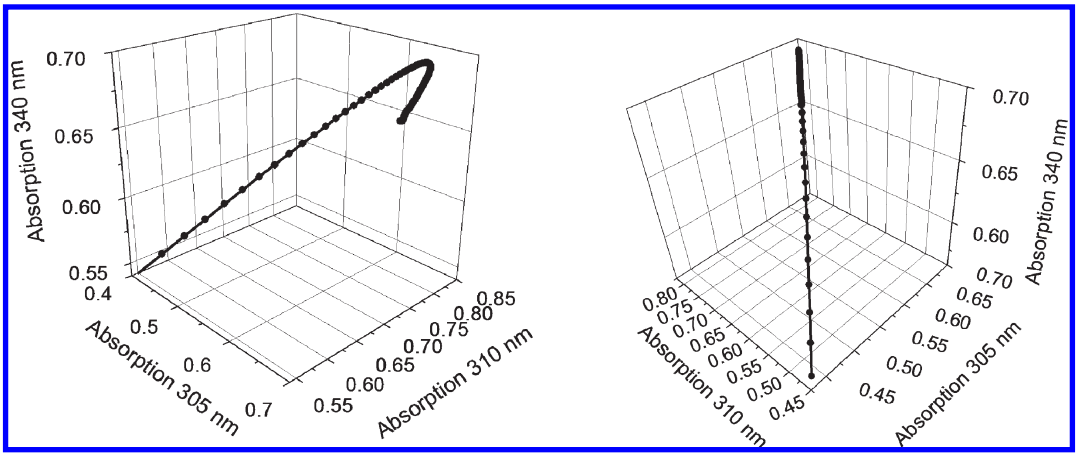

Figure 9. (a) Three-dimensional absorption−absorption−absorption correlations and (b) projection.

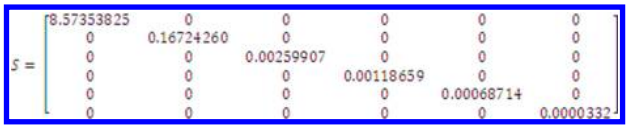

Figure 10. Diagonal matrix S indicating two singular values.

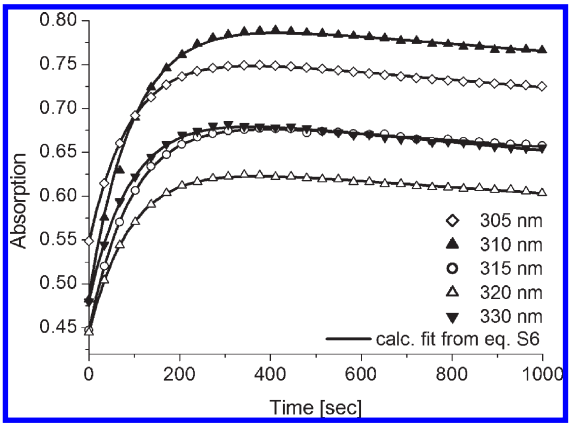

Figure 11. Measured and calculated extinction curve at 315 nm with $A_0 = 1.8 \times 10^{-4}$ M.

The concentration curves shown in Figure 12 were obtained by implementing the obtained coefficients into the differential equation system shown in Supporting Information equations S2−S4.

Catalytic Performance of Compound 4. The isolated orange material described above for which we have good evidence that is represents compound $[ReO_3(L^{tBu})]$ (**4**) was investigated as catalyst in the oxidation of *cis*-cyclooctene. Identical reaction conditions were applied as in the experiment with catalyst **2** (in chloroform at 50 °C, 1 mol % catalyst, 2 equiv of TBHP). The progress of the reaction was monitored by GC-MS analysis. Comparing the performance of compound **4** to that of **2** showed very similar results: after 0.25 h 23% (28% with **2**), after 4 h 35% (42% with **2**), and after 24 h 50% (56% with **2**). This provides further evidence that the rhenium(V) catalyst precursor is converted to **4**, which is responsible for the catalytic conversion of the olefin to the epoxide.

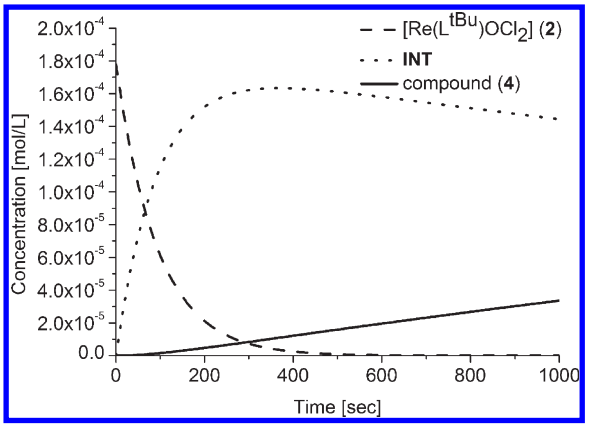

Figure 12. Species distribution curves of compounds **2**, **INT**, and **4**.

CONCLUSION

In this work the straightforward synthesis of a series of Re^V complexes bearing novel tridentate pyridazine-containing ligands is presented. X-ray crystallography of complexes **1** and **2** revealed a rare *trans*-dichloro oxo configuration at the rhenium centers. Complexes **1**−**3** were fully characterized including NMR and IR spectroscopy as well as EI mass spectrometry and cyclic voltammetry. They were successfully applied in the catalytic oxidation of cyclooctene with TBHP, yielding ~60% cyclooctene oxide after 24 h. Furthermore, we could clearly show that the initial precatalyst **2** is converted to **4** via one intermediate **INT**. This supports our proposal where **2** quickly reacts to **INT** (presumably $[ReO_2(L^{tBu})]$), which is subsequently slowly converted to $[ReO_3(L^{tBu})]$ (**4**) (eq 1). The constants obtained for formation of **INT** and the obtained rate constant of the epoxidation process deviate several orders of magnitude. Thus, neither **2** nor **INT** is the catalytically active species. The rate-determining step represents formation of compound **4**, which is the entry point into the catalytic cycle.

EXPERIMENTAL SECTION

General Considerations. Substituted hydrazinopyridazines[27] and $[ReOCl_3(OPPh_3)(SMe_2)]$[28] were prepared according to literature procedures. All other chemicals were purchased from commercial sources and used without further purification. All NMR spectra were

dx.doi.org/10.1021/ic200756r |*Inorg. Chem.* 2011, 50, 7162–7171

measured on a Bruker Avance III spectrometer (300 MHz for ^{1}H and 75 MHz for ^{13}C NMR). The ^{1}H NMR spectroscopic data are reported as s = singlet, d = doublet, t = triplet, m = multiplet or unresolved, and br = broad signal, coupling constant(s) are given in Hertz, and shifts are given in ppm relative to the solvent residual peak. Infrared spectra were measured on a Bruker ALPHA-P Diamant ATR-FTIR spectrometer. Mass spectroscopy was performed on an Agilent Technologies 5973D inert XL MSD direct insertion probe spectrometer applying electron impact ionization. GC-MS analyses were performed on an Agilent 7890A with an Agilent 19091J-433 column coupled to a spectrometer-type Agilent 5975C. UV/vis spectra were acquired with a Varian Cary 50 spectrophotometer with a thermostatted cuvette holder.

X-ray Diffraction Analyses. Intensity data sets for compounds **1** and **2** were collected using a Bruker Smart Apex II diffractometer equipped with a graphite monochromator (Mo Kα radiation, λ = 0.71073 Å) and a CCD detector. Compound **1** was measured at 100 K, whereas compound **2** showed a disruptive phase transition upon cooling and was therefore measured at 293 K. The structures were solved by direct methods (SHELXS-97) and refined by full-matrix least-squares techniques against F^2 (SHELXL-97). Although systematic absences and intensity statistics seemed to indicate for complex **2** the presence of a glide plane *m*, a meaningful solution could only be found for the noncentrosymmetric space group $Pna2_1$ (no. 33) instead of the apparent *Pnma* (no. 63). All non-hydrogen atoms were refined with anisotropic displacement parameters. Data were corrected for absorption and *Lp* factors with SADABS.[59] Hydrogen atoms were placed geometrically and refined using a riding model. CCDC 809604 (for **1**) and 809605 (for **2**) contain the supplementary crystallographic data for this paper. These data can be obtained free of charge from the Crystallographic Data Centre via www.ccdc.cam.ac.uk/data_request/cif.

Electrochemical Methods. Redox chemical properties of complexes **1**−**3** were carried out in an argon-filled glovebox using a Gamry Reference 600 potentiostat connected to a personal computer. Cyclic voltammograms were obtained in 0.05 M solution $[^nBu_4N][PF_6]$/CH_3CN at 25 °C. The experiments were carried out in a three-electrode glass cell with a platinum disk (d = 3 mm) working electrode, a platinum wire auxiliary electrode, and a [$Ag/AgNO_3$ 0.01 M in CH_3CN, 0.1 M $[^nBu_4N][ClO_4]$] reference electrode. Under these conditions, oxidation of ferrocene occurs at 0.095 V.

General Procedure for Ligand Syntheses. A suspension of para substituted 3-(1-methylhydrazino)pyridazine (1 equiv) in ethanol (100 mL) was heated to reflux. Salicylaldehyde (1 equiv) was added to the resulting solution. A white precipitate started to form after a few minutes. The reaction mixture was heated to reflux for an additional 10 h, after which full conversion was evidenced by TLC. After cooling the solution to room temperature the white precipitate was filtered off and washed with ice-cooled ethanol to give pure products.

Synthesis of HL^{tol}. General synthesis using 3-(1-methylhydrazino)-6-(4-*para*-methylphenyl)pyridazine (500 mg, 2.33 mmol) and salicylaldehyde (285 mg, 249 μL, 2.33 mmol) afforded 735 mg (99%) of pure $\mathbf{HL^{tol}}$. ^{1}H NMR (300 MHz, DMSO-d_6, 298 K): δ 2.35 (s, 3H, CH_3), 3.76 (s, 3H, NCH_3), 6.87−6.95 (m, 2H, Ar*H*), 7.21 (m, 1H, Ar*H*), 7.30 (d, J = 8.1 Hz, 1H, Ar*H*), 7.81 (m, 1H, Ar*H*), 7.87 (d, J = 9.5 Hz, 1H, Ar*H*), 7.96 (d, J = 8.1 Hz, 2H, Ar*H*), 8.00 (d, J = 9.5 Hz, 1H, Ar*H*), 8.16 (s, 1H, N=C*H*), 10.17 (s, 1H, O*H*). ^{13}C NMR (75 MHz, DMSO-d_6, 298 K): δ 21.3 (CH_3), 30.1 (N−CH_3), 115.4, 116.6, 119.9, 121.7, 126.1, 126.2, 126.9, 129.9, 130.5, 133.9, 135.2, 139.0, 152.8, 156.3, 158.4 (imino and aromatic carbons).

Synthesis of HL^{tBu}. General synthesis using 3-(1-methylhydrazino)-6-(4-*tert*-butyl)pyridazine (500 mg, 2.77 mmol) and salicylaldehyde (339 mg, 296 μL, 2,77 mmol) afforded 710 mg (90%) of pure $\mathbf{HL^{tBu}}$. ^{1}H NMR (300 MHz, DMSO-d_6, 298 K): δ 1.33 (s, 9H, C−(CH_3)$_3$), 3.70 (s, 3H, NCH_3), 6.87−6.93 (m, 2H, Ar*H*), 7.18 (m, 1H, Ar*H*), 7.64 (d, J = 9.5 Hz, 1H, Ar*H*), 7.76 (d, J = 9.3 Hz, 2H, Ar*H*), 8.11 (s, 1H, N=C*H*), 10.26 (s, 1H, O*H*). ^{13}C NMR (75 MHz, DMSO-d_6, 298 K): δ 30.1 (C−(CH_3)$_3$), 30.3 (C−(CH_3)$_3$), 36.5 (N−CH_3), 115.3, 116.6, 119.8, 121.7, 125.9, 127.0, 130.3, 134.8, 156.2, 158.0, 163.5 (imino and aromatic carbons).

Synthesis of HL^{Cl}. General synthesis using 3-(1-methylhydrazino)-6-(4-chloro)pyridazine (500 mg, 3.15 mmol) and salicylaldehyde (385 mg, 336 μL, 3.15 mmol) afforded 760 mg (92%) of pure $\mathbf{HL^{Cl}}$. ^{1}H NMR (300 MHz, DMSO-d_6, 298 K): δ 3.68 (s, 3H, NCH_3), 6.84−6.95 (m, 2H, Ar*H*), 7.20 (m, 1H, Ar*H*), 7.67 (d, J = 9.5 Hz, 1H, Ar*H*), 7.81 (d, J = 7.5 Hz, 1H, Ar*H*), 7.96 (d, 1H, Ar*H*), 8.16 (s, 1H, N=C*H*), 10.12 (s, 1H, O*H*). ^{13}C NMR (75 MHz, DMSO-d_6, 298 K): δ 30.2 (N−CH_3), 116.6, 118.7, 119.8, 121.6, 126.6, 130.2, 130.8, 135.6, 148.6, 156.4, 159.1 (imino and aromatic carbons).

Synthesis of [$ReOCl_2(L^{tol})$] (1). $\mathbf{HL^{tol}}$ (100 mg, 0.31 mmol) and [$ReOCl_3(OPPh_3)(SMe_2)$] (199 mg, 0.31 mmol) were suspended in acetone (20 mL) and heated to 50 °C. After a few seconds, a color change to red occurred and the reagents slowly dissolved. The resulting clear deep red solution was evaporated to dryness. Recrystallization from hot acetonitrile afforded 145 mg (78%) of pure **1** as red crystals suitable for X-ray diffraction analysis. ESI-MS (m/z (%)): 590 $[M]^+$ (60); 556 $[M - Cl]^+$ (100); 521 $[M - :Cl_2]^+$ (85). ^{1}H NMR (300 MHz, DMSO-d_6, 298 K): δ 2.09 (s, 3H, CH_3), 4.01 (s, 3H, NCH_3), 7.21 (m, 1H, Ar*H*), 7.44 (d, J = 8.1 Hz, 2H, Ar*H*), 7.52 (m, 2H, Ar*H*), 7.80 (d, J = 9.7 Hz, 1H, Ar*H*), 7.93 (d, J = 7.6 Hz, 1H, Ar*H*), 8.16 (d, J = 8.1 Hz, 2H, Ar*H*), 8.28 (s, 1H, N=C*H*), 8.45 (d, J = 9.7 Hz, 1H Ar*H*,). ^{13}C NMR (75 MHz, DMSO-d_6, 298 K): δ 21.5 (CH_3), 34.9 (N-CH_3), 100.0, 111.8, 114.8, 119.0, 119.6, 126.8, 130.4, 131.4, 1834.1, 135.2, 140.9, 147.0, 152.6, 156.7, 164.7 (imino and aromatic carbons). IR: (cm^{-1}, ATR) 1707 (m), 1599 (m), 1499 (s), 961 (s, ν_{as} Re=O), 805 (s), 760 (s), 620 (m). Anal. Calcd for $ReC_{19}H_{17}N_4O_2Cl_2$ (Found): C, 38.65 (38.06); H, 2.90 (2.91); N, 9.49 (9.45).

Synthesis of [$ReOCl_2(L^{tBu})$] (2). $\mathbf{HL^{tBu}}$ (100 mg, 0.78 mmol) and [$ReOCl_3(OPPh_3)(SMe_2)$] (223 mg, 0.78 mmol) were suspended in acetone (20 mL) and heated to 50 °C. After a few seconds, a color change to red occurred and the reagents slowly dissolved. The resulting clear deep red solution was evaporated to dryness. Recrystallization from dichloromethane afforded 125 mg (64%) of pure **2** as red crystals suitable for X-ray diffraction analysis. ESI-MS (m/z (%)): 556 $[M]^+$ (100); 522 $[M - Cl + H]^+$ (95); 486 $[M - Cl_2]^+$ (25). ^{1}H NMR (300 MHz, DMSO-d_6, 298 K): δ 1.46 (s, 9H, C−(CH_3)$_3$), 3.95 (s, 3H, NCH_3), 7.18 (m, 1H, Ar*H*), 7.21 (d, J = 9.7 Hz, 1H, Ar*H*), 7.50 (m, 2H, Ar*H*), 7.91 (m, 1H, Ar*H*), 8.22 (s, 1H, N=C*H*), 8.34 (d, J = 9.7, 1H, Ar*H*). ^{13}C NMR (75 MHz, DMSO-d_6, 298 K): δ 29.2 (C−(CH_3)$_3$), 29.6 (C−(CH_3)$_3$), 37.4 (N−CH_3), 111.9, 114.6, 118.8, 119.6, 132.8, 133.9, 135.1, 146.5, 156.4, 163.6, 164.6 (imino and aromatic carbons). IR (cm^{-1}, ATR): 1600 (s), 1505 (s), 1435 (m), 1363 (m), 1149 (m), 982 (s), 964 (s, ν_{as} Re=O), 763 (s). Anal. Calcd for $ReC_{16}H_{19}N_4O_2Cl_2$ (Found): C, 34.54 (34.65); H, 3.44 (3.43); N, 10.07 (10.12).

Synthesis of [$ReOCl_2(L^{Cl})$] (3). $\mathbf{HL^{Cl}}$ (100 mg, 0.38 mmol) and [$ReOCl_3(OPPh_3)(SMe_2)$] (241 mg, 0.38 mmol) were suspended in acetone (20 mL) and heated to 50 °C. After a few seconds, a color change to red occurred and the reagents slowly dissolved. The resulting clear deep red solution was evaporated to dryness. Recrystallization from hot acetonitrile afforded 170 mg (83%) of pure **3** as red crystals. ESI-MS (m/z (%)): 534 $[M]^+$ (80); 500 $[M - Cl + H]^+$ (100); 465 $[M - Cl_2]^+$ (30). ^{1}H NMR (300 MHz, DMSO-d_6, 298 K): δ 4.00 (s, 3H, NCH_3), 7.24 (m, 1H, Ar*H*), 7.42 (d, J = 9.7 Hz, 1H, Ar*H*), 7.53 (m, 2H, Ar*H*), 7.94 (d, J = 7.8 Hz, 1H, Ar*H*), 8.31 (s, 1H, N=C*H*), 8.45 (d, J = 9.7, 1H, Ar*H*). ^{13}C NMR (75 MHz, DMSO-d_6, 298 K): δ 35.3 (N-CH_3), 111.49, 117.0, 119.2, 119.6, 134.4, 135.5, 135.7, 147.3, 148.2, 157.1, 164.8 (imino and aromatic carbons). IR (cm^{-1}, ATR): 1594 (m), 1504 (s), 1394 (m), 1296 (m), 1151 (m), 982 (m), 963 (s, ν_{as} Re=O), 821 (m), 771 (s), 708 (m), 466 (m). Anal. Calcd for $ReC_{16}H_{19}N_4O_2Cl_2$ (Found): C, 26.95 (26.76); H, 1.88 (1.84); N, 10.48 (10.36).

Synthesis of [$ReO_3(L^{tBu})$] (4). To a solution of complex **2** (20 mg, 36 μmol) in chloroform (2 mL) was added TBHP (5.5 M solution in decane, 75 μL, 360 μmol). The mixture was heated to 50 °C and stirred for 8 h. Subsequently, all volatiles were removed under reduced pressure to yield a pale orange material, which was triturated with diethyl ether for 10 min to remove most of the decane. The material could as yet not be obtained in an analytically pure form. ^{1}H NMR (300 MHz, DMSO-d_6, 298 K): δ 1.37 (s, 9H, C−(CH_3)$_3$), 4.35 (s, 3H, NCH_3), 7.06 (t, J = 7.5 Hz, 1H, ArH_{Ph}), 7.13 (d, J = 8.1 Hz, 1H, ArH_{Ph}), 7.61 (m, 2H, ArH), 8.48 (d, J = 9.9 Hz, 1H, ArH_{Pdz}), 8.96 (d, J = 9.9 Hz, 1H, ArH_{Pdz}), 10.50 (s, 1H, N=CH). IR (cm^{-1}, ATR): 1369 (w), 1130 (w), 888 (vs), 828 (w), 759 (w).

Catalytic Investigations. In a typical experiment catalyst (10 μmol) and substrate (1 mmol) were dissolved in $CHCl_3$ (2 mL) at 50 °C. To start the reaction ^{t}BuOOH 5.5 M in decane (363 μL, 2 mmol) was added. Immediately a sample (10 μL) was taken to mark the initial concentration. GC-MS sampling (10 μL) was repeated periodically. Decane was used as the internal standard for quantification.

For the catalytic UV−vis experiment catalyst [$ReOCl_2(L^{tBu})$] (**2**) (1 g of a 300 μM stock solution in $CHCl_3$, 0.2 μmol) was diluted with chloroform (2 g) in the quartz cuvette. After addition of cyclooctene (26 μL of a 10 wt % solution, 2.2 mg, 20 μmol), the cuvette was placed into the thermostatted cuvette holder (50 °C) of the spectrophotometer. The catalytic reaction was started by adding TBHP (5.5 M in *n*-decane, 72 μL, 800 μmol). Every 5 min a UV−vis spectrum was acquired. Periodically, a sample for GC-MS analysis was taken (10 μL). Decane was used as the internal standard for quantification.

For the UV−vis experiment for mechanistic investigations a stopped flow instrument equipped with thermostatted sample reservoirs was connected to the spectrophotometer, all heated to 50 °C. It was loaded with solutions of complex **2** (300 μM, 1 equiv) and TBHP (5.7 mM, 19 equiv) in chloroform. The solutions were combined directly in the cuvette, which initiated data collection. Every 8 s a UV−vis spectrum was acquired.

■ ASSOCIATED CONTENT

Supporting Information. Molecular view of complex **2** and processing details for graphical and mathematical assessment. This material is available free of charge via the Internet at http://pubs.acs.org.

■ AUTHOR INFORMATION

Corresponding Author
*E-mail: nadia.moesch@uni-graz.at.

■ ACKNOWLEDGMENT

The authors acknowledge Forte−Wissenschafterinnenkolleg FreChe Materie for financial support.

■ REFERENCES

(1) Romao, C. C.; Kühn, F. E.; Herrmann, W. A. *Chem. Rev.* **1997**, *97*, 3197–3246.
(2) Jain, K. R.; Herrmann, W. A.; Kühn, F. E. *Coord. Chem. Rev.* **2008**, *252*, 556–568.
(3) Kühn, F. E.; Santos, A. M.; Herrmann, W. A. *Dalton Trans* **2005**, *15*, 2483–2491.
(4) Beattie, I. R.; Jones, P. J. *Inorg. Chem.* **1979**, *18*, 2318–2319.
(5) Owens, G. S.; Arias, J.; Abu-Omar, M. M. *Catal. Today* **2000**, *55*, 317–363.
(6) Kühn, F. E.; Groarke, M. In *Applied Homogeneous Catalysis with Organometallic Compounds*. Cornils, B., Herrmann, W. A., Eds.; Wiley-VCH: Weinheim, Germany, 2002; pp 1304−1318.
(7) Yudin, A. K.; Sharpless, K. B. *J. Am. Chem. Soc.* **1997**, *119*, 11536–11537.
(8) Adam, W.; Mitchell, C. M. *Angew. Chem., Int. Ed.* **1996**, *35*, 533–535.
(9) Copéret, C.; Adolfsson, H.; Sharpless, K. B. *Chem. Commun.* **1997**, 1565–1566.
(10) Xu, Z.; Zhou, M. D.; Drees, M.; Chaffey-Millar, H.; Herdtweck, E.; Herrmann, W. A.; Kühn, F. E. *Inorg. Chem.* **2009**, *48*, 6812–6822.
(11) Gonzales, J. M.; Distasio, R., JR.; Periana, R. A. *J. Am. Chem. Soc.* **2007**, *129*, 15794–15804.
(12) Thiel, W. R. *Angew. Chem., Int. Ed.* **2003**, *42*, 5390–5392.
(13) Du, G.; Abu-Omar, M. M. *Curr. Org. Chem.* **2008**, *12*, 1185–1198.
(14) Nolin, K. A.; Ahn, R. W.; Toste, F. D. *J. Am. Chem. Soc.* **2005**, *127*, 12462–12463.
(15) Lippert, C. A.; Soper, J. D. *Inorg. Chem.* **2010**, *49*, 3682–3684.
(16) Espenson, J. H. *Coord. Chem. Rev.* **2005**, *249*, 329–341.
(17) Sachse, A.; Mösch-Zanetti, N. C.; Lyashenko, G.; Wielandt, J. W.; Most, K.; Magull, J.; Dall'Antonia, F.; Pal, A.; Herbst-Irmer, R. *Inorg. Chem.* **2007**, *46*, 7129–7135.
(18) Schröckeneder, A.; Traar, P.; Raber, G.; Baumgartner, J.; Belaj, F.; Mösch-Zanetti, N. C. *Inorg. Chem.* **2009**, *48*, 11608–11614.
(19) Traar, P.; Schröckeneder, A.; Judmaier, M. E.; Belaj, F.; Baumgartner, J.; Sachse, A.; Mösch-Zanetti, N. C. *Eur. J. Inorg. Chem.* **2010**, *36*, 5718–5727.
(20) Dinda, S.; Drew, M. G. B.; Bhattacharyya, R. *Catal. Commun.* **2009**, *10*, 720–724.
(21) Deloffre, A.; Halut, S.; Salles, L.; Bregeault, J.-M.; Gregorio, J. R.; Denise, B.; Rudler, H. *Inorg. Chem.* **1999**, *17*, 2897–2898.
(22) Kühn, F. E.; Rauch, M. U.; Lobmaier, G. M.; Artus, G. R. J.; Herrmann, W. A. *Chem. Ber.* **1997**, *130*, 1427–1431.
(23) Lobmaier, G. M.; Frey, G. D.; Dewhurst, R. D.; Herdtweck, E.; Herrmann, W. A. *Organometallics* **2007**, *26*, 6290–6299.
(24) Herrmann, W. A.; Rauch, M. U.; Artus, G. R. J. *Inorg. Chem.* **1996**, *35*, 1988–1991.
(25) Jacobsen, E. N.; Zhang, W.; Muci, A. R.; Ecker, J. R.; Deng, L. *J. Am. Chem. Soc.* **1991**, *113*, 7063–7064.
(26) Yang, J. Y.; Nocera, D. G. *J. Am. Chem. Soc.* **2007**, *129*, 8192–8198.
(27) Grünwald, K. R.; Saischek, G.; Volpe, M.; Belaj, F.; Mösch-Zanetti, N. C. *Eur. J. Inorg. Chem.* **2010**, *15*, 2297–2305.
(28) McPherson, L. D.; BeReau, V. M.; Abu-Omar, M. M.; Ugrinova, V.; Pu, L.; Taylor, S. D.; Brown, S. N. *Inorg. Synth.* **2004**, *34*, 54–59.
(29) Machura, B.; Kruszynski, R.; Jaworska, M. *Polyhedron* **2006**, *25*, 1111–1124.
(30) Inego, E.; Zangrando, E.; Mestroni, S.; Fronzoni, G.; Stener, M.; Alessio, E. *Dalton Trans.* **2001**, 1338–1346.
(31) Schmid, S.; Strähle, J. *Z. Kristallogr.* **1992**, *198*, 49–59.
(32) Lock, C. J. L.; Turner, G. *Can. J. Chem.* **1977**, *55*, 333.
(33) Gerber, T. I. A.; Tshentu, Z. R.; Garcia-Granda, S.; Mayer, P. *J. Coord. Chem.* **2003**, *56*, 1093–1103.
(34) Wittern, U.; Strähle, J.; Abraham, U. *Z. Anorg. Allg. Chem.* **1997**, *623*, 218–223.
(35) Banerjee, S.; Bhattacharyya, S.; Dirghangi, B. K.; Menon, M.; Chakravorty, A. *Inorg. Chem.* **2000**, *39*, 6–16.
(36) Xu, L.; Setyawati, I. A.; Pierreroy, J.; Pink, M.; Young, V. G., Jr.; Patrick, B. O.; Rettig, S. J.; Orvig, C. *Inorg. Chem.* **2000**, *39*, 5958–5963.
(37) Abu-Omar, M. M.; Khan, S. I. *Inorg. Chem.* **1998**, *37*, 4979–4985.
(38) Lis, T. *Acta Crystallogr.* **1976**, *B32*, 2707–2709.
(39) Machura, B.; Wolff, M.; Kusz, J.; Kruszynski, R. *Polyhedron* **2009**, *28*, 2949–2964.
(40) Videira, M.; Silva, F.; Paulo, A.; Santos, I. C. *Inorg. Chim. Acta* **2009**, *362*, 2807–2813.
(41) Connelly, N. G.; Geiger, W. E. *Chem. Rev.* **1996**, *96*, 899–910.

(42) Herrmann, W. A.; Fischer, R. W.; Scherer, W.; Rauch, M. U. *Angew. Chem., Int. Ed.* **1993**, *32*, 1157–1160.
(43) Al-Ajlouni, A.; Espenson, J. H. *J. Am. Chem. Soc.* **1995**, *117*, 9243–9250.
(44) Espenson, J. H. *Chem. Commun.* **1999**, 479–488.
(45) Pipes, D. W.; Meyer, T. J. *Inorg. Chem.* **1986**, *25*, 3256–3262.
(46) Brewer, J. C.; Gray, H. B. *Inorg. Chem.* **1989**, *28*, 3334–3336.
(47) Parker, D.; Roy, P. S. *Inorg. Chem.* **1988**, *27*, 4127–4130.
(48) Shan, X.; Ellern, A.; Guzei, I. A.; Espenson, J. H. *Inorg. Chem.* **2003**, *42*, 2362–2367.
(49) Machura, B.; Kruszynski, R.; Penczek, R.; Mrozinski, J.; Kusz, J. *Polyhedron* **2008**, *27*, 797–804.
(50) Machura, B.; Dziegielewski, J. O.; Kruszynski, R.; Bartczak, T. J. *J. Coord. Chem.* **2004**, *57*, 1–7.
(51) Barz, M.; Rauch, M. U.; Thiel, W. R. *Inorg. Chem.* **1997**, 2155–2161.
(52) Okuda, J.; Herdtweck, E.; Herrmann, W. A. *Inorg. Chem.* **1988**, *27*, 1254–1257.
(53) Mauser, H. *Formale Kinetik*; Bertelsmann Verlag: Düsseldorf, Germany, 1974.
(54) Mauser, H. *Z. Naturforsch.* **1968**, *23b*, 1025–1030.
(55) Polster, J.; D., H. *Phys. Chem. Chem. Phys.* **2001**, *3*, 993–999.
(56) Hugus, Z. Z., Jr.; El-Awady, A. A. *J. Phys. Chem.* **1971**, *75*, 2954–2957.
(57) Maeder, M.; Zuberbühler, A. D. *Anal. Chem.* **1990**, *62*, 2220–2224.
(58) Chau, F. T.; Mok, K. W. *Computers Chem.* **1992**, *16*, 239–242.
(59) Bruker, AXS. *SADABS V2008-1*; Bruker: Madison, WI, 2008.